Controlling the Position and Orientation of Single Silver Nanowires on a Surface Using Structured Optical Fields

Zijie Yan,[†] Julian Sweet,[‡] Justin E. Jureller,[†] Mason J. Guffey,[†] Matthew Pelton,[‡] and Norbert F. Scherer[†,‡,*]

[†]The James Franck Institute, The University of Chicago, 929 East 57th Street, Chicago, Illinois 60637, United States and [‡]Center for Nanoscale Materials, Argonne National Laboratory, 9700 South Cass Avenue, Argonne, Illinois 60439, United States

ABSTRACT

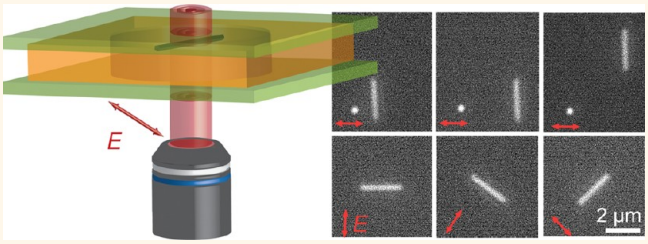

We demonstrate controlled trapping and manipulation of single silver (Ag) nanowires in two dimensions at a surface using structured light fields generated with a spatial light modulator. The Ag nanowires are attracted toward the regions of maximal optical intensity along the surface when the trapping laser light is linearly polarized and are repelled toward the minima of optical intensity when the light is circularly polarized. For linearly polarized light, stably trapped nanowires are oriented perpendicular to the polarization direction due to a torque induced by an asymmetrical response of the nanowire to the electric field. The attractive interactions with linearly polarized trapping laser light, which is at 800 nm for all measurements, enable stable trapping and translation of Ag nanowires in the antinodes of optical gratings and in zero-order Bessel beams. Trapped nanowires can be positioned and oriented on a transparent dielectric substrate, making possible the nonmechanical assembly of plasmonic nanostructures for particular functions.

KEYWORDS: optical tweezers · Ag nanowires · optical manipulation · plasmonics · structured light

Plasmonic metal nanowires are envisioned to serve as key components in nano-optical systems, allowing optical fields to be relayed over distances of several micrometers while being confined on the nanoscale in transverse directions.[1−4] In particular, chemically synthesized silver (Ag) nanowires are nearly free of bulk crystalline defects and thus offer plasmon transport that is limited only by intrinsic losses in the metal.[1,2,5] This property of Ag nanowires has been exemplified by integration with single-photon sources, wherein the emission from a single quantum dot is coupled with tunable efficiency to a Ag nanowire.[6] Interactions between Ag nanoparticles and Ag nanowires,[7] and between branched Ag nanowires,[1,3] allow local coupling of plasmons into and out of the wires. The ability to tailor the time-dependent phase of optical pulses allows for spatial focusing and localization of plasmonic wave packets in these wires,[8,9] which may enable sensing and nonlinear optics applications.[10] Ultimately, these applications as well as other advances would benefit from a method to accurately position and orient individual metal nanowires on a surface without using mechanical methods, such as scanning probes,[11] that could damage the wires.

Optical forces have the potential to serve as a noncontact method for single-nanowire manipulation. So far, optical tweezers have been used to trap semiconductor nanowires,[12,13] metal nanoparticles,[14−19] and nanorods.[20−22] However, optical trapping of plasmonic nanowires that are free to move in three dimensions still remains a challenge. One obstacle to trapping Ag nanowires is the strong radiation pressure in the beam propagation direction. This can be ameliorated by restricting the manipulation to a surface, as recently demonstrated by Tong *et al.*[23] They found that Ag nanowires in linearly polarized Gaussian beam tweezers could be oriented perpendicular to the laser polarization, while nanowires in circularly polarized tweezers tended to rotate. However, controllable translation of the nanowires along the surface was not demonstrated,[23] suggesting that the trapped nanowires were partially held in place due to nonspecific chemical interactions with the surface[24,25] rather than solely due to optical forces. In addition, the reported results do not clearly indicate how linearly polarized light maintains the orientation of a Ag nanowire or how that orientation is related to the spatial profile of the trapping field.

* Address correspondence to nfschere@uchicago.edu.

Received for review June 24, 2012 and accepted August 9, 2012.

Published online August 17, 2012
10.1021/nn302795j

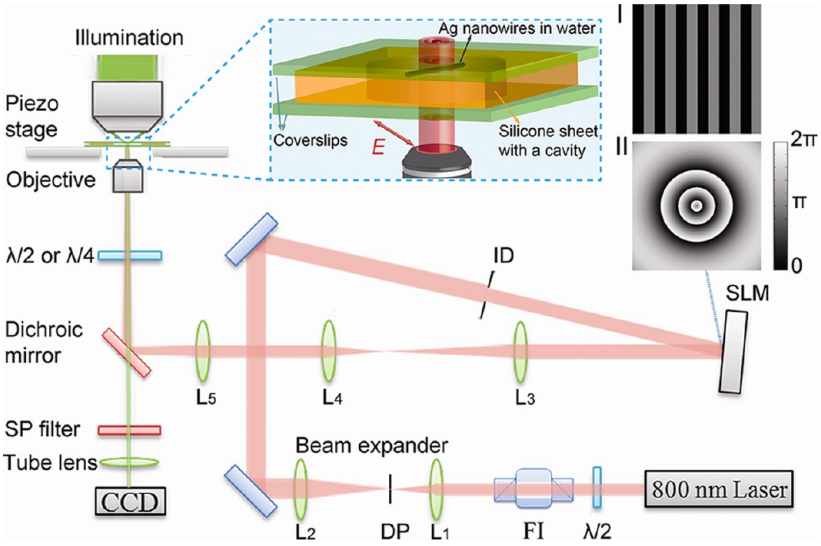

Figure 1. Schematic of the experimental setup. SLM, spatial light modulator; ID, iris diaphragm; DP, diamond pinhole; FI, Faraday isolator; SP filter, short-pass filter (cutoff = 650 nm); $\lambda/2$, half-waveplate; $\lambda/4$, quarter-waveplate. Focal lengths of the lenses: L_1, 15 cm; L_2, 40 cm; L_3, 75 cm; L_4, 20 cm; L_5, 50 cm. Insets at the top right show the phase masks used to generate (I) the grating pattern and (II) the Bessel beam.

Achieving complete control over the position and orientation of Ag nanowires in two dimensions (2D) requires an understanding of the magnitude and direction of optical gradient forces acting along the surface. Studies of plasmonic nanoparticles and nanorods have shown that attractive forces, toward the maxima of optical intensity, only occur if the laser wavelength is greater than the plasmon resonance wavelengths; otherwise, the optical forces are repulsive and the nanostructures are pushed toward the minima of optical intensity.[15−17,20,26] Ag nanowires support a single transverse plasmon resonance, excited by light polarized perpendicular to their long axis, and with a frequency close to that of spherical Ag nanoparticles. They also support multiple longitudinal plasmon resonances, excited by light polarized parallel to their long axis, and with resonance frequencies whose spacing decreases as the lengths and aspect ratio of the nanowire increase.[27,28] The longitudinal plasmon modes are similar to the resonances of a Fabry−Pérot cavity: a series of overlapping peaks that cover the frequency range from the visible to the near-infrared region.[5,9] Optical forces on a Ag nanowire are thus expected to be dependent on the wavelength and polarization of the light, and experiments are needed to provide insight into the nature of these optical forces.

In this paper, we study the interaction of Ag nanowires with various structured light fields in two dimensions. Structured light fields provide the strong optical gradients that are necessary for trapping,[26] while still allowing the entire Ag nanowire to be illuminated. This is in contrast to a tightly focused Gaussian beam, which we have found does not result in robust trapping of Ag nanowires, probably because of the small spatial overlap with the long wires. The structured light fields thus provide stronger and more controllable optical forces than a Gaussian spot, enabling us to demonstrate controllable optical orientation and positioning of single Ag nanowires on a transparent substrate.

RESULTS AND DISCUSSION

The experiments were conducted using the optical-tweezers apparatus illustrated in Figure 1. Briefly, a spatial light modulator (SLM) was used to generate structured light fields at the focus of a microscope objective. These fields were used to trap and manipulate the Ag nanowires shown in Figure 2. Radiation pressure from the trapping beam pushes the nanowires up against the surface of a glass coverslip, so that motion of the nanowires is restricted to two dimensions. Details of the sample preparation and trapping apparatus are provided in the Methods section.

Interaction of Ag Nanowires with an Optical Grating. Longitudinal plasmon modes of Ag nanowires are excited only by light incident on the ends of the wires;[5] optical forces on the wires are thus expected to depend on the spatial extent of the trapping field relative to the length of the wire. We therefore studied the motion of Ag nanowires in an optical grating pattern that has a total illumination area of about $10.5 \times 9.5\ \mu m^2$. This large illumination area makes it possible to exert optical gradient forces without explicitly choosing an illumination position along the wire. The optical grating is extended in one direction and modulated sinusoidally in the perpendicular direction. This pattern was generated by the SLM using a phase mask that consists of two interlaced regions that shift the phase of the wavefront by 0 and π (Figure 1, inset I).

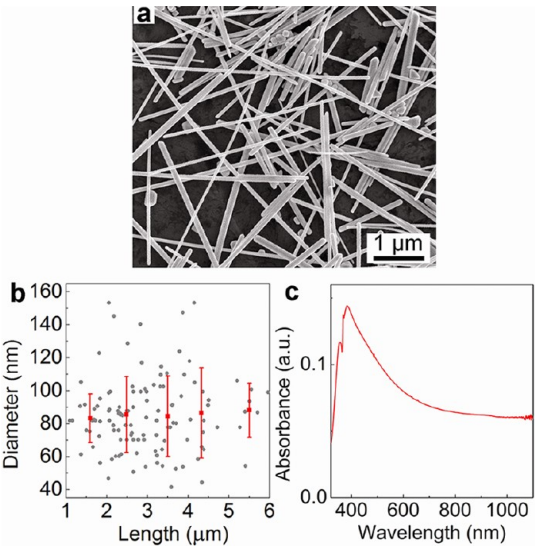

Figure 2. (a) Scanning electron microscopy (SEM) image of the Ag nanowire sample used in the experiments. (b) Sizes of the nanowires with lengths from 1 to 6 μm. Gray circles are dimensions of individual nanowires measured from SEM images. The red squares are mean diameters for nanowires categorized according to their length, with a bin size of 1 μm, and the error bars are standard deviations about these means. (c) Absorption spectrum of an ensemble of Ag nanowires in water. The continuous absorbance tail at longer wavelengths results from the inhomogeneous distribution of longitudinal resonances that are strongly dependent on the lengths and diameters of the Ag nanowires.[2]

Figure 3a shows representative dark-field images of a Ag nanowire (length of 2.6 μm) in the grating pattern for different polarizations of the optical field. Two-dimensional trajectories of the centroid of the Ag nanowire and histograms of the centroid positions are shown in Figure 3b–e. In this paper, the horizontal direction of an image is defined as the *x*-direction, and the vertical direction is the *y*-direction. The polarization direction is characterized by the angle, θ, relative to the *x*-direction, and we define the nanowire orientation, δ, as the angle of the long axis of the nanowire relative to the *x*-direction. Finally, the optical axis for propagation of the trapping beam is along the *z*-axis (*i.e.*, along the surface normal).

The trajectories of the nanowire positions show that the optical interactions depend strongly on polarization. If the light is linearly polarized, the Ag nanowire is always oriented with its long axis perpendicular to the polarization direction. Of particular interest is the case when the polarization is perpendicular to the long axis of the bright fringes of the optical grating (*i.e.*, $\theta = 0°$): the nanowire is then stably trapped in the center of a bright fringe.

When the angle between the polarization and the direction of the grating stripes was decreased (*i.e.*, as θ changed from 0 to $-45°$), the trap stability was lost, and the nanowire wandered throughout the pattern. As seen in the histograms of Figure 3c,d, the centroid of the nanowire is more likely to reside in the dark regions of the optical grating than in the bright regions for $\theta = -45$ and $-90°$. This suggests that the ends of the nanowire are attracted toward the bright regions of the trap; as illustrated in Figure 4a, placing the centroid of the wire in the middle of a dark fringe maximizes the overlap of the ends of the wires with the optical field.

The fraction of the wire length covered by the bright region of the grating also affects its orientational stability. The standard deviation of the nanowire orientation was the smallest when the nanowire was fully covered by a bright region (see Figure 4b). For the wire shown in Figure 3, when $\theta = -45°$, the standard deviation of the nanowire orientation was smaller when the centroid of the nanowire was in the dark regions and its ends were in the bright regions (see Figure 4c). When $\theta = -90°$, the fraction of the wire illuminated by the grating is similar for the centroid in the bright region or in the dark region, and the orientational stability is also similar in the two cases (see Figure 4d).

When the light is circularly polarized, the nanowire spins (see Figure 3a,IV) due to the transfer of spin angular momentum.[29] The nanowire is also repelled from the regions of maximum intensity of the optical grating and quickly moves into an adjacent minimum of optical intensity (see Figure 3e). While in this dark region, the wire diffuses out of the illuminated pattern altogether, indicating that linear polarization is essential for stable optical trapping of Ag nanowires. Several other Ag nanowires were studied in the optical grating and they all exhibited behaviors similar to the nanowire in Figure 3; an additional example is shown in Figures S1 and S2 of the Supporting Information.

The measured position and orientation distributions can be used to calculate an effective trapping potential (potential of mean force). Assuming that the distributions of wire position *x*, *y* and orientation δ are independent, the potential of mean force, pmf(α), is given by

$$\mathrm{pmf}(\alpha) = -k_B T \ln P(\alpha) \quad (1)$$

where k_B is Boltzmann's constant, *T* is absolute temperature, and $P(\alpha)$ is the probability density of the parameter α (*x*, *y*, or δ). Figure 5a shows the trapping potentials of Ag nanowires in an optical grating, with zero potential set to the minimum of pmf(α). (Note that determining the depth of the potential requires measurements of many (>100) escape (or capture) events. Our focus was to illustrate the robustness of the nanowire trapping, which requires multiple measurements on the same nanowire, and therefore, we cannot report absolute depths.) The potential in the *x*-direction has a well-defined minimum for $\theta = 0°$ (case I) and increases by approximately $2k_BT$ for a displacement of 200 nm from the equilibrium position. For $\theta = -90°$ (case III), the potential in the *x*-direction does not have a well-defined minimum, indicating the lack of stable trapping. By contrast, the potentials in the *y*-direction are similar for the different polarization directions (Figure 5b),

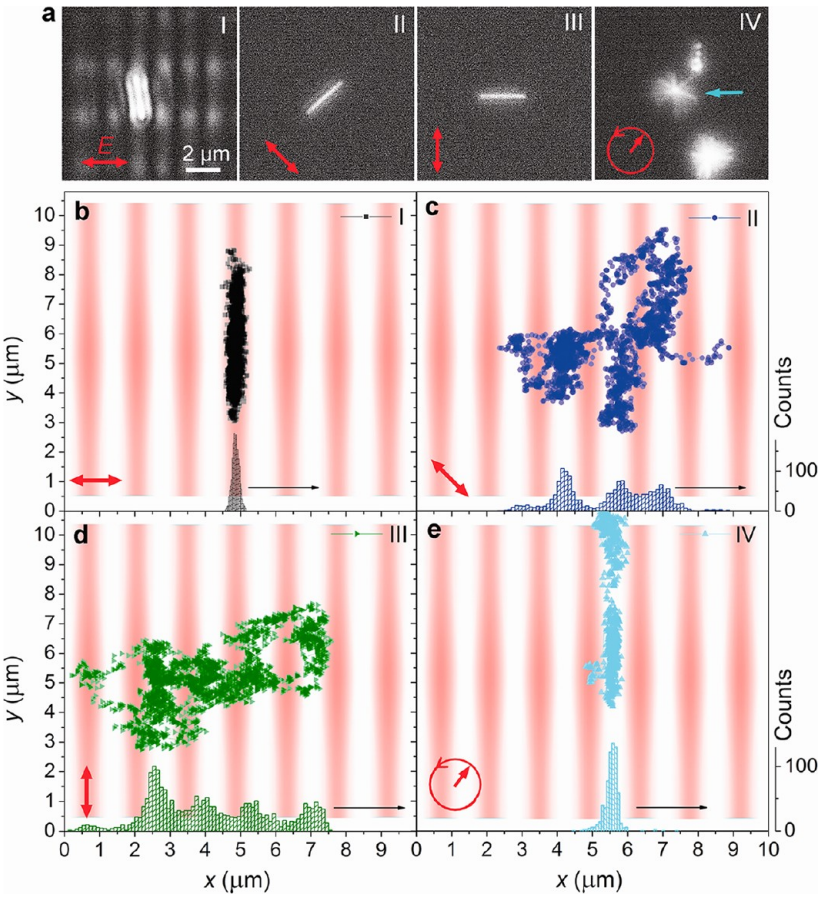

Figure 3. (a) Single Ag nanowire in an optical grating pattern. The laser pattern can be seen in I but is not visible in II−IV because a short-pass filter was inserted before the camera. We note that nodes are observed along the *y*-direction in a.I. These nodes are imaging artifacts, due to thin-film interference effects from coated optics in the microscope; we have verified that they do not correspond to variations in the illumination intensity. On the other hand, the illumination does have a small gradient of intensity in the *y*-direction, inherited from the Gaussian profile of the laser beam that illuminates the SLM. The polarization of the laser beam is linear in I−III with the direction indicated by the red arrow (I, $\theta = 0 \pm 4°$; II, $\theta = -45 \pm 4°$; III, $\theta = -90 \pm 4°$) and it is circular in IV. The image shown in IV is a superposition of 12 frames, covering a total time of 0.2 s, illustrating the rotation of nanowires. The image contains a particle and two nanowires; the cyan arrow indicates the nanowire that is the same as in I−III (see Supporting Information, movie S1). (b−e) Trajectories of the centroid of the Ag nanowire as a function of time, with the laser polarization corresponding to that shown in (a). The red stripes in the background represent the bright fringes of the laser pattern. Histograms of the centroid position are shown at the bottom of each panel (b−e). The time step in the trajectories is 1/60 s.

corresponding to the Gaussian intensity profile in the *y*-direction, inherited from the laser beam incident on the SLM. The potential well for δ is narrower for $\theta = 0°$ than for $\theta = -90°$ (Figure 5c), indicating better control over the orientation of the nanowire when the polarization was perpendicular to the long axis of the bright fringes.

The bright fringes could also trap other nanowires with different lengths, generally in the range of 1−3 μm. Figure 6 shows the position and orientation stability of trapped Ag nanowires as a function of their length. The position stability is independent of the length of the wire since the trapped wires are always shorter than the bright fringes and are thus always exposed to the same optical fields in the fringes. This also suggests that the important wire−field interaction does not change with the wire length, and thus the lateral position confinement is dominantly due to the field interacting with the transverse plasmon mode of the wire.

In contrast, the orientational stability of longer nanowires is greater than that of shorter nanowires; this indicates that either the total torque that the light exerts on the wire in order to maintain orientation stability is proportional to the wire length or the efficacy of thermal noise decreases with increasing moment of inertia. Finally, it is worth noting that the position and orientation stability of a trapped nanowire depends on the laser power, and the nanowire trapping is more stable when the power is higher (see Figures S3 and S4 in the Supporting Information).

The optical grating can simultaneously trap and align multiple nanowires in separate fringes, as shown in Figure 7a. If multiple wires are trapped, they prefer to remain in separate fringes rather than associate in one fringe. We note that, during the measurement, nanowire 1 hopped from the fringe where it was originally trapped into an adjacent fringe, which already held

nanowire 2. When this occurred the wires preferred to minimize their side-to-side overlap in the fringe. That is, this pair (and other pairs not shown) exhibits a repulsive interaction when caught in the same fringe. The calculated trapping potential using the position distributions of these nanowires is shown in Figure 7b.

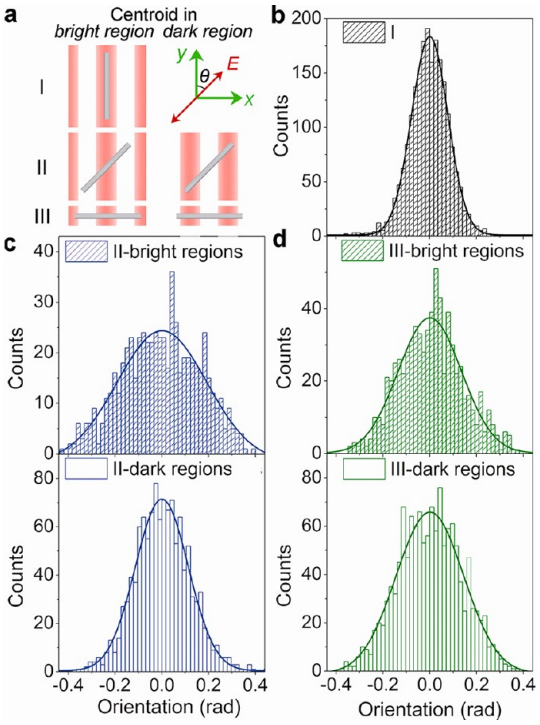

Figure 4. (a) Schematics of the possible positions of the centroid of a nanowire relative to the bright or dark regions of an optical grating, for different polarizations of the trapping light. A half-width of the sinusoidal period around the maximum intensity of a bright fringe is defined as the bright region, and the other half is the dark region. (b–d) Histograms and corresponding Gaussian fits of the orientation of the nanowire in the grating pattern with respect to the *y*-direction. In (b), $\theta = 0°$ and the standard deviation of the nanowire orientation $\sigma = 0.077$ rad; in (c), $\theta = -45°$ and $\sigma = 0.192$ rad for the top panel (when the centroid is located in a bright region) and $\sigma = 0.113$ rad for the bottom panel (when the centroid is located in a dark region); and in (d), $\theta = -90°$ and $\sigma = 0.136$ rad for the top panel (bright regions) and $\sigma = 0.145$ rad for the bottom panel (dark regions). Panels (b), (c), and (d) correspond to cases I–III, respectively, illustrated in Figure 3a and panel (a).

The potential well shows periodic minima, corresponding well to the optical grating structure. Movie S3 in the Supporting Information shows that, when the pattern is translated in the *x*- or *y*-direction, multiple nanowires would move simultaneously to maintain their positions in the bright fringes.

Numerical Simulations of Optical Forces on Ag Nanowires. To understand why the nanowire is oriented perpendicular to the optical polarization, we performed three-dimensional electrodynamics simulations using the finite-difference time-domain (FDTD) method; see the Methods section for additional details. As shown in Figure 8a,l, a Ag nanowire is situated in the $x-y$ plane and is illuminated by uniform planewaves propagating along the *z*-axis with different polarizations, θ, relative to the short axis of the wire. Planewave illumination is chosen in order to ensure that any orientation effects are due to the polarization of the light and not due to optical gradients. Figure 8b shows the calculated

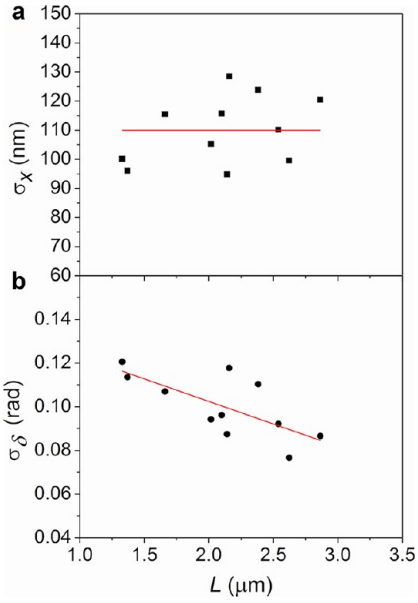

Figure 6. Trap stiffness *vs* nanowire length. (a) Standard deviation of the displacement along the *x*-axis (σ_x) and (b) standard deviation of the orientation (σ_δ) of a Ag nanowire trapped in an optical grating with $\theta = 0°$. Red lines are linear fits of the data.

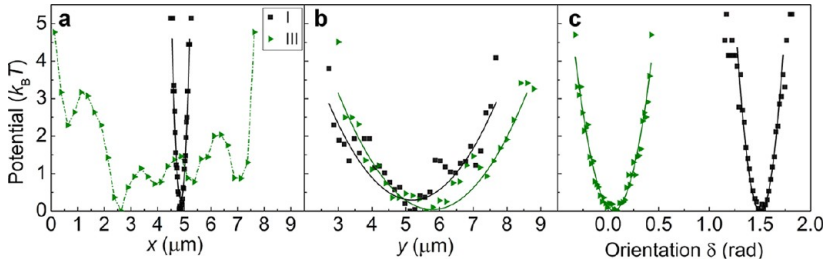

Figure 5. Trapping potentials for Ag nanowires in an optical grating for (a) the *x*-direction, (b) the *y*-direction, and (c) orientation. Potentials are shown for (I) polarization perpendicular to the *y*-direction ($\theta = 0°$, black squares) and (III) polarization parallel to the *y*-direction ($\theta = -90°$, green triangles), corresponding to the cases shown in Figure 3b,d, respectively. Solid curves are parabolic fits of the data; the dashed line for case III in panel (a) is a guide for the eye.

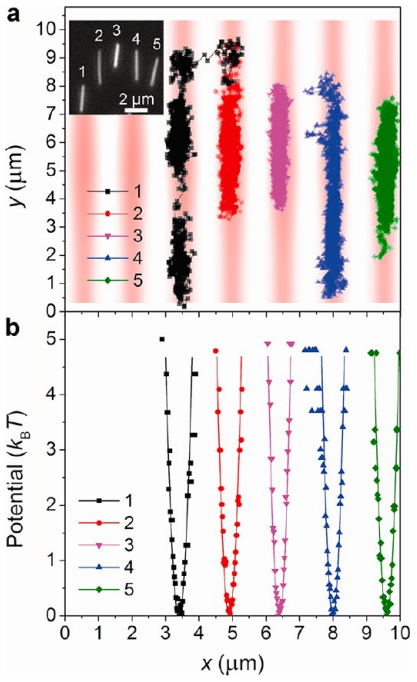

Figure 7. (a) Trajectories of five Ag nanowires simultaneously trapped by an optical grating pattern with $\theta = 0°$. The time step in the trajectories is 1/60 s (see Supporting Information, movie S2). The inset shows an optical image of the nanowires. (b) Trapping potentials in the *x*-direction for Ag nanowires in the optical grating. Solid curves are parabolic fits of the data. Nanowire 1 hopped from one fringe to another late in the measurement. We have omitted these data from the lower panel to avoid confusion due to the small number of samples after the hop.

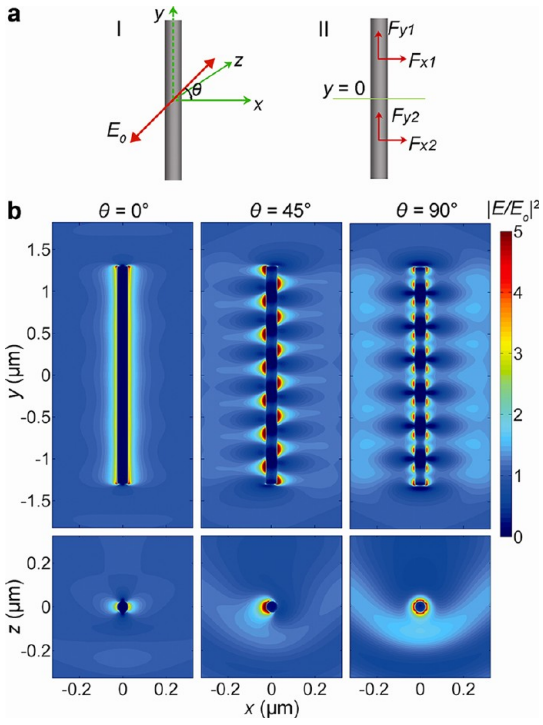

Figure 8. (a,I) Illustration of the coordinate system used in the three-dimensional finite-difference time-domain (FDTD) simulations. (a,II) Optical forces on the top and bottom parts of a nanowire (D = 50 nm, L = 2.6 μm along the y-axis) illuminated by a linearly polarized planewave with wavelength of 800 nm propagating in the z-direction. (b) Planar representations of the simulated intensity of the electric field, E, around the Ag nanowire, relative to the incident field E_o; $|E/E_o|^2$. Results are shown for the incident planewave with different polarization directions, θ, relative to the x-direction. The top panels are cross sections of the nanowire in the x–y plane at z = 0, and the bottom panels are cross sections of the x–z plane at y = 80 nm.

electric-field intensity distributions around a nanowire. When $\theta = 0°$, the 800 nm light interacts nonresonantly with the transverse mode; when $\theta = 90°$, it excites a high-order longitudinal plasmon mode. In both of these cases, the local electric field is symmetric with respect to the y–z plane at $x = 0$. However, when $0 < \theta < 90°$, the light excites a superposition of the transverse and longitudinal modes, resulting in an asymmetric local field around the nanowire; this is illustrated in Figure 8b for $\theta = 45°$. The asymmetric interaction with and response to the field generates an asymmetric optical force, or a torque, on the nanowire.

We estimate the torque by separating the nanowire into two equal regions along its length and separately calculating the optical forces on the two halves of the wire by integrating the Maxwell stress tensor (MST). The results are shown in Table 1; each value has been normalized by the total incident intensity and the area over which the forces are applied. F_{x1} and F_{x2} have different signs for $\theta = 45°$, corresponding to a net torque on the wire. We assume that the optical force for each half of the wire acts on the center of the corresponding segment, so that the net torque is $\tau_{45} = (F_{x1} - F_{x2}) \times D \times L/2 \times L/4 = -7.2$ pN·μm/W. The torque will rotate the wire toward $\delta = -45°$, at which point the torque is zero and the orientation of the wire is stable (equivalent to the configuration of $\delta = 90$ and $\theta = 0°$). The torque is also zero for $\theta = 90°$, but this position is metastable and easily disrupted by thermal fluctuations. At $\theta = 5°$, $\tau_5 = -1.3$ pN·μm/W; the restoring potential for an optical power of 100 mW is thus $U = \tau_5 \times \theta_f = 2.7 k_BT$ for a rotation of $\theta_f = -0.087$ rad from $\theta = 5°$ to $\theta = 0°$. This is in reasonable agreement with curve I of Figure 5c, which gives a potential difference of approximately k_BT for a rotation of $\theta_f = -0.087$ rad. Note that, in all cases, $F_x = F_{x1} + F_{x2} = 0$ and $F_y = F_{y1} + F_{y2} = 0$, so the position of the nanowire is stable in the x–y plane, and $F_z > 0$, corresponding to radiation pressure in the beam propagation direction.

Table 1 also shows calculated forces for a nanowire illuminated by a focused Gaussian beam, with the center of the beam displaced 50 nm toward the left side of the wire from its center. For $\theta = 0°$, $F_x = F_{x1} + F_{x2} < 0$, indicating that the center of the wire is attracted toward the bright spot. A larger beam focus results in a larger attractive force, indicating that the total force is proportional to the fraction of the wire covered by the light. This last result is consistent with the observation in Figure 3 that the nanowire tends to maximize its

TABLE 1. Calculated Optical Forces on the Ag Nanowire (D = 50 nm, L = 2.6 μm; Positive Values Indicate Repulsive Forces and Negative Values Indicate Attractive Forces)

light field	light field center (μm, μm)	illumination area (x–y plane) (μm × μm)	θ (deg)	F_{x1} (pN/(μm^2·W))	F_{x2} (pN/(μm^2·W))	F_{y1} (pN/(μm^2·W))	F_{y2} (pN/(μm^2·W))	F_{z1} (pN/(μm^2·W))	F_{z2} (pN/(μm^2·W))
planewave	(0, 0)	0.65 × 3.65	0	0	0	11	−11	25	25
			5	−15	15	11	−11	28	28
			45	−85	85	−34	34	223	223
			90	0	0	−80	80	422	422
Gaussian beam	(−0.05, 0)	0.65 × 1	0	−5	−5	4	−4	16	16
			45	−55	94	−17	17	128	128
		0.65 × 2	0	−10	−10	5	−5	36	36

overlap with the optical field. On the other hand, for θ = 45°, the total force on the wire in the x-direction is repulsive. There is also a torque in this case that acts to orient the nanowire toward δ = −45°, indicating that wires in a tightly focused Gaussian beam will be oriented perpendicular to the polarization of the light, as in a planewave. However, this orientation must be achieved before the nanowire is repelled from the Gaussian beam in order for stable trapping to be possible. Therefore, weak trapping and orientational control of the nanowires is possible with focused Gaussian beams, but the trapping is more tenuous than with extended fields.

The optical forces calculated for incident planewaves are shown as a function of wavelength in Figure 9, together with the calculated absorption spectra. For θ = 0°, there is a large absorption peak at 370 nm due to excitation of the transverse plasmon resonance, and the radiation pressure also has a maximum at this wavelength due to the strong absorption. At θ = 90°, multiple longitudinal plasmon resonances are excited, which also produce maxima in the radiation pressure. At θ = 45°, the absorption spectrum and the radiation pressure correspond to a combination of the spectra for θ = 0 and 90°. The torque, which only exists for θ = 45° (or 0° < θ < 90°), is counterclockwise for all wavelengths from 740 to 820 nm, including the laser wavelength of 800 nm of the present experiments. However, the simulation predicts that the torque will change direction when the wavelength passes through a longitudinal plasmon resonance. The sign of the gradient force is expected to change when passing through a resonance; in particular, it has been observed that gradient forces on nanoparticles with an isolated plasmon resonance are attractive for trapping laser wavelengths on the red side of the resonance when the polarization of the particle is in phase with the applied field and is repulsive for laser wavelengths on the blue side of the resonance when the polarization of the particle is out of phase with the applied field.[20,26] The situation is more complex for nanowires, where there are multiple, closely spaced plasmon resonances, since the laser frequency will always be on the red side of some resonances and on the blue side of others. The net force depends on the competition between these

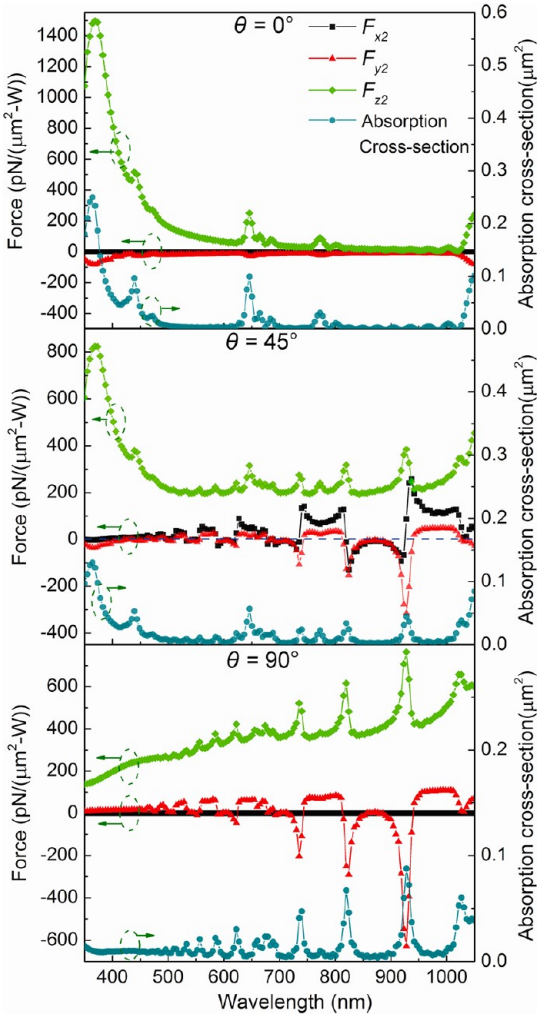

Figure 9. Optical forces and absorption cross sections for a Ag nanowire, calculated using FDTD simulations, for an incident planewave with different polarization directions, θ, relative to the short axis of the wire. The Cartesian components of the force F_{x2} (black), F_{y2} (red), and F_{z2} (green) and the absorption cross section (cyan) are shown for three values of θ. The blue dashed line in the second panel indicates zero force. The values of F_{x1} and F_{y1}, not shown here, are the negatives of the values of F_{x2} and F_{y2}, respectively, and values of F_{z1} are equal to the values of F_{z2}.

resonances, which results in the predicted changes in orientation direction. The calculation indicates, for example, that the nanowire should be oriented parallel to the polarization for wavelengths between 820 and 870 nm. Similarly, the net torque is nearly zero at 870 nm, indicating that orientational control over the nanowire will be lost at this wavelength. Verifying the predicted wavelength dependence of the nanowire orientation will be the subject of future investigations. Nonetheless, the calculations strongly suggest that the ability of optical fields to orient and position silver nanowires is closely tied to the excitation of plasmonic resonances in the wires.

Optical Trapping and Manipulation of Ag Nanowires Using Bessel Beams. The calculation results described above suggest that optical trapping of a Ag nanowire in a tightly focused Gaussian beam may be difficult, due to the need for orientation to occur more rapidly than repulsion from the beam and due to the limited overlap between the beam and the length of the wire. Indeed, we found experimentally that Ag nanowires could be manipulated (*e.g.*, oriented) by a focused Gaussian beam only if the nanowires were weakly held by (presumably) a polymer tether to the surface, in which case translation of the nanowires was not possible. Together with the successful results for the sinusoidal grating potential, this suggest that stable optical trapping and manipulation of the nanowires requires a light field with greater spatial extent in the lateral direction along the surface, but still with sufficiently strong gradients to provide trapping forces that are significant compared with thermal fluctuations.

In addition to the sinusoidal grating field described above, zero-order Bessel beams (ZOBBs) meet these requirements. A ZOBB can be generated by passing a Gaussian beam through an axicon[30] or by imposing an equivalent phase profile using an SLM. However, the maximum intensity of the central spot of the ZOBB occurs a short distance from the SLM,[31] complicating the optical setup. We therefore shifted the intensity maximum to the image plane by adding a Fresnel lens phase mask to the axicon phase mask on the SLM. The total phase mask used is shown in inset II of Figure 1, and the resulting ZOBB is shown in Figure 10a. The diameter of the central spot is about 1 μm, and that of the first and second rings are about 2.1 and 3.8 μm, respectively.

Individual Ag nanowires were stably trapped in this ZOBB trap, as shown in Figure 10b. This required careful adjustment of the laser power: if it is too high, then the trapped nanowires adhere to the surface within a few seconds; if it is too low, then the radiation pressure is insufficient to push the nanowires against the surface and upward against gravity. As discussed in the Supporting Information, the Bessel beam is expected to induce significantly more heating of the nanowire than the optical grating pattern; this heating is likely responsible for adhesion of the nanowires to the glass surface when the power is too high. We therefore decreased the laser power from 100 mW for the optical grating to 50 mW for the Bessel beam.

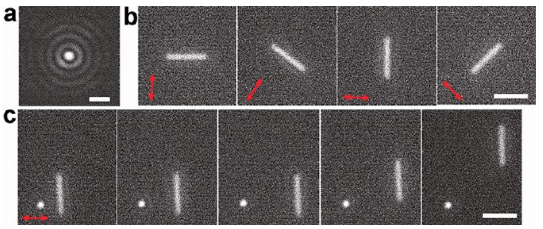

Figure 10. Trapping with a zero-order Bessel beam (ZOBB). (a) Image of the cross section of the ZOBB. (b) Alignment of a Ag nanowire trapped near a glass surface by the ZOBB for different polarizations of the trapping light, indicated with the red arrows. (c) Translation of a nanowire trapped by the ZOBB relative to a fixed nanoparticle (bright dot) stuck on the surface. The scale bars are 2 μm (see Supporting Information, movie S4).

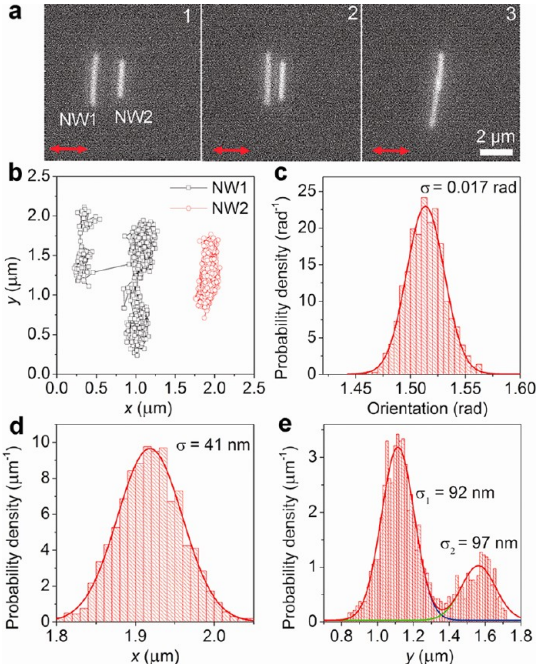

Figure 11. Multiple nanowire trapping in the ZOBB trap. (a) Dark-field images of two Ag nanowires trapped near a glass surface by the linearly polarized ZOBB (see Supporting Information, movie S5). In panel 1, the first nanowire (NW1) is trapped by the second ring of the ZOBB, and the second one (NW2) is trapped by the central spot (located at $x = 1.9$ μm, $y = 1.5$ μm). In panel 2, NW1 is trapped by the first ring, and NW2 is still trapped by the central spot. In panel 3, both nanowires are trapped by the central spot. (b) Trajectories of the two trapped nanowires for the time interval between panels 1 and 2 of (a). The time step for the trajectory is 1/60 s. (c–e) Histograms and corresponding Gaussian fits of the orientation, the *x*-position, and the *y*-position, respectively, of NW2 trapped by the central spot.

The nanowires typically became trapped when their centers were in the ZOBB trap. Trapping of the ends of a nanowire was also possible but occurred less frequently. As in the optical gratings, the trapped nanowires became oriented perpendicular to the linear polarization of the trapping field, as shown in

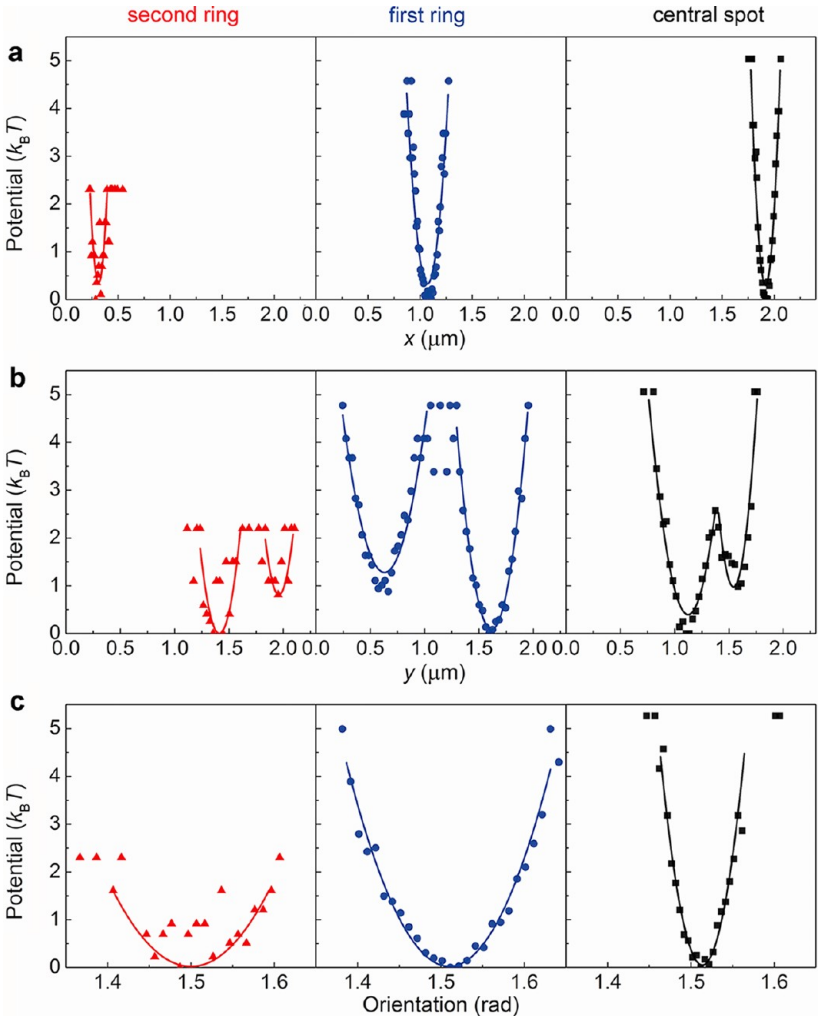

Figure 12. Trapping potentials of mean force for a Ag nanowire in the linearly polarized ZOBB for (a) the *x*-direction, (b) the *y*-direction, and (c) orientation. From left to right, the panels show potentials of mean force for a wire trapped in the second ring of the ZOBB (calculated using the data for NW1 of Figure 11), a wire trapped in the first ring (NW1), and a wire trapped in the central spot (NW2). Quadratic fits to the data are also shown.

Figure 10b. Figure 10c shows translation of the trapped nanowire relative to a stationary Ag nanoparticle on the surface. (Such nanoparticles existed in the solution as a byproduct of the nanowire synthesis, and they could also be easily trapped by the ZOBB trap.) These results demonstrate that the ZOBB trap permits arbitrary 2D positioning and orientation of individual Ag nanowires near surfaces.

As well as being trapped in the central spot of the ZOBB, nanowires could be trapped by the side rings. This permitted simultaneous trapping of multiple nanowires, as shown in Figure 11a. The freedom of motion of the nanowires is exemplified by the ability to controllably translate them along the surface and also by spontaneous fluctuations of nanowire position within the trap. Figure 11b exhibits the trajectories of the two nanowires while they are trapped in separate parts of the ZOBB. The first nanowire (NW1) spontaneously hopped between two rings and eventually hopped into the central spot, where the second nanowire (NW2) was located. The orientation of NW2 had a standard deviation of 1°, as shown in Figure 11c, indicating more stable orientational trapping than in the optical grating. The standard deviation of the nanowire displacement along its short axis is 42 nm, as seen in Figure 11d. However, it is less stable along the long axis and moved between two trapping positions, as shown in Figure 11e. Movie S5 in the Supporting Information shows that both of the nanowires could be translated and rotated simultaneously.

Trapping potentials of mean force were calculated for the ZOBB in the same way as for the grating patterns. As shown in Figure 12a, the central spots and rings produce well-defined trapping minima in the *x*-direction. The central spot has a deeper potential than the first ring, which, in turn, has a deeper potential than the second ring, reflecting the diminishing intensities of the concentric rings. The same trend is seen for the orientational potentials, as shown in Figure 12c. Figure 12b shows that the minima of the potential in

the *y*-direction occur near the beam center. Since the potentials are calculated from the probability density of the centroids of the nanowires, this indicates that the nanowires are most likely to be trapped at their midpoints.

To verify that linear polarization is essential for optical trapping of Ag nanowires, we also tried to trap Ag nanowires using the ZOBB with circular polarization. In this case, the nanowires spun around their own axes and wandered randomly through the Bessel beam (see Supporting Information, movie S6).

The optical grating is extended in one direction and can thus illuminate the entire length of the Ag nanowires. This means, though, that the optical gradient is weak in this direction; in addition, changing the orientation of nanowires trapped in a grating would require simultaneously rotating the grating pattern and the optical polarization. In contrast, the Bessel beam can illuminate only a portion of the nanowires but provides stronger local gradients and allows the nanowire orientation to be changed simply by rotating the polarization of the incident light. An extension of the ZOBB allows for three-dimensional trapping of Ag nanowires, which we will report elsewhere. A common feature of the two optical fields is that they can both be considered as resulting from the interference of planewaves: an ideal optical grating results from the superposition of two planewaves propagating at an angle to one another, and an ideal zero-order Bessel beam is a superposition of planewaves propagating on a cone.[30] We thus expect that there are many other interfering optical fields that could trap and manipulate Ag nanowires on a surface.

CONCLUSIONS

We have demonstrated that Ag nanowires can be stably oriented and positioned on a surface using optical forces. Using an optical grating pattern with light wavelength of 800 nm, we show that the optical gradient force on Ag nanowires is attractive when the light is linearly polarized and repulsive when the light is circularly polarized. In linearly polarized light, the nanowires are oriented perpendicular to the polarization direction. This orientation is explained by calculations showing that, if the polarization is oriented in a different direction, asymmetric local fields are produced around the nanowire, resulting in a net torque. The calculations also suggest that the trap stability and the nanowire orientation relative to the polarization direction might change if one changes the trap wavelength, which will be a topic for further experimental investigations. Since the optical grating was produced by a spatial light modulator, the fringe position, orientation, and period can be rapidly changed simply by changing the phase mask on the SLM. This will make it possible to translate nanowires along the surface and to sort them from one another or from other nanoparticles based on the strength of their optical interactions.[32]

We have studied two structured optical fields: optical gratings and zero-order Bessel beams. A linearly polarized zero-order Bessel beam could exert strong attractive forces on plasmonic Ag nanowires, and adjusting the beam polarization direction could readily orient single Ag nanowires on a transparent substrate. We expect that the same should occur for other materials. In preliminary experiments, we have found that the zero-order Bessel beam could be used to also manipulate Au nanowires of various lengths (2−3 μm) on surfaces by the zero-order Bessel beam. These wires exhibit the same orientation−polarization relationship as the Ag nanowires.

The demonstrated positional and orientational control opens up the possibility of controllably depositing plasmonic nanowires on a substrate and assembling integrated nanophotonic and plasmonic circuits. It may be possible to deposit the nanowires simply by increasing the laser power, producing stronger radiation pressure and increased local heating. Alternatively, the nanowires may be fixed on a substrate using appropriate chemical functionalization of both surfaces[33,34] or using photocurable polymers.[25] Such deposition and assembly is the subject of ongoing research.

METHODS

Ag Nanowires. Ag nanowires were synthesized *via* the polyol reduction of $AgNO_3$.[35] The nanowire lengths ranged from approximately 1 to 20 μm, and the diameters were approximately 50−150 nm. The synthesized nanowires were washed with acetone (to remove polyvinylpyrrolidone, a surfactant used in the polyol synthesis, from the nanowire surface) and deionized water, purified by centrifugation, and redispersed thoroughly in deionized water.

Optical Tweezers. The optical tweezer apparatus was constructed using a home-built Ti:sapphire laser operating at a wavelength of 800 nm and output power of approximately 400 mW.[33] The linearly polarized laser output passes through a Faraday optical isolator, and is spatially filtered and collimated, resulting in a symmetric Gaussian beam with a diameter of 12 mm. This beam illuminates a phase-only spatial light modulator (SLM; X10468 Series, Hamamatsu Photonics) which is used to generate the programmed structured light fields used in this report. Three relay lenses direct the shaped beam to an inverted microscope (Olympus IX71). The beam is reflected off a short-pass dielectric dichroic mirror and is focused using a 60× water immersion objective (NA 1.2, Olympus UPLSAPO). When linearly polarized light is used, a rotatable half-waveplate placed before the objective is used to adjust the polarization direction. When circularly polarized light is used, this half-waveplate is replaced by a quarter-waveplate. The waveplates are placed after the dichroic mirror in order to avoid difficulties due to the polarization dependence of reflectance from this dielectric reflector. The laser power in the sample cell was measured to be approximately 100 mW when the grating pattern was used and was adjusted to approximately 50 mW when the Bessel beam was used.

Sample Cell. The sample cell for the microscopy experiments was constructed using a silicone sheet spacer (approximately 130 μm in thickness) placed between two coverslips (no. 1.5, Fisher Scientific). The spacer had a circular cavity with diameter of 6 mm. The coverslips were cleaned with acetone and deionized

water and were then treated with ozone and ultraviolet light to minimize the possibility that the Ag nanowires adhere to their surfaces. The spacer was first put on one coverslip, water containing the nanowires was dropped into the cavity, and the cell was then covered by the other coverslip. The silicone spacer forms a seal that prevents evaporation and retains the water between the coverslips for at least several hours. The nanowires settle down to the bottom of the sample cell, but the sedimentation occurs very slowly, on time scales much longer than the duration of the experiment (*e.g.*, 2 h). The cell was mounted on a closed-loop piezoelectric stage (PI P-561 with E-710 digital piezo controller) that can move in three dimensions with an accuracy of 1 nm. Nanowires in the cell were imaged using dark-field microscopy, with the dichroic mirror and an additional short-pass filter used to remove scattered laser light. The nanowires that were imaged were at the water−glass surface of the top coverslip in the sample cell; during the trapping experiments, the nanowires were held against this glass surface due to radiation pressure from the trapping beam. Images and videos of the nanowires were recorded using a Firewire camera (Sony XCD-V60).

Image Analysis. The position and orientation of nanowires were extracted from the optical images and videos using custom software written in Matlab. Briefly, the software applies a convolution kernel to filter the original image[36] and then uses the built-in Matlab "edge" function to detect the nanowires. The grayscale image is converted into a binary image, and the "regionprops" function is used to extract the centroid position and orientation of the detected nanowires. Additional objects in the image, such as the small surface-stuck nanoparticle seen in Figure 10, were eliminated based on their lengths and/or eccentricities.

Electrodynamic Simulations. Electric-field distributions and optical forces were obtained from three-dimensional finite-difference time-domain (FDTD) calculations using the commercial software package "FDTD Solutions" (Lumerical, Inc.). The Ag nanowire was approximated as a solid circular cylinder with a diameter of 50 nm and a length of 2.6 μm. The dielectric function of Ag was modeled with parameters adjusted to match tabulated values from ref 37, and the background refractive index was set to be 1.33 (the infinite-frequency refractive index of water). The Ag nanowire was illuminated by a linear polarized light source with a wavelength of 800 nm, which was modeled either as a planewave or a Gaussian beam with waist radius of 1 μm and waist location at the position of the wire. The simulation region is $0.65 \times 0.65 \times 3.65$ μm^3, and a non-uniform mesh with maximum grid size of 3 nm was used. Optical forces on the nanowire were calculated by integrating the Maxwell stress tensor over a surface surrounding the nanowire. The absorption cross sections were calculated as $\sigma_{abs}(\omega) = P_{abs}(\omega)/I_{inc}(\omega)$, where P_{abs} is the total power absorbed by the nanowire and I_{inc} is the incident intensity.

Conflict of Interest: The authors declare no competing financial interest.

Acknowledgment. We acknowledge support from the U.S. Department of Energy (DOE), Office of Science, Division of Chemical, Geological and Biological Sciences under Contract No. DE-AC02-06CH11357, and acknowledge the NSF CCI program and the UC Irvine CaSTL center (CHE-0802913) for funds to acquire the 2D SLM used in this research. This work was also supported in part by the National Science Foundation (CHE-1059057). We also used the University of Chicago NSF-MRSEC (DMR-0820054) central facilities for nanowire characterization. Use of the Center for Nanoscale Materials was supported by the U.S. Department of Energy (DOE), Office of Science, Office of Basic Energy Sciences, under Contract No. DE-AC02-06CH11357.

Supporting Information Available: Movie clips showing the optical manipulation processes, additional figures showing the Ag nanowire−optical grating interactions, and estimation of heating effects. This material is available free of charge *via* the Internet at http://pubs.acs.org.

REFERENCES AND NOTES

1. Sanders, A. W.; Routenberg, D. A.; Wiley, B. J.; Xia, Y.; Dufresne, E. R.; Reed, M. A. Observation of Plasmon Propagation, Redirection, and Fan-Out in Silver Nanowires. *Nano Lett.* **2006**, *6*, 1822–1826.
2. Wild, B.; Cao, L.; Sun, Y.; Khanal, B. P.; Zubarev, E. R.; Gray, S. K.; Scherer, N. F.; Pelton, M. Propagation Lengths and Group Velocities of Plasmons in Chemically Synthesized Gold and Silver Nanowires. *ACS Nano* **2012**, *6*, 472–482.
3. Fang, Y.; Li, Z.; Huang, Y.; Zhang, S.; Nordlander, P.; Halas, N. J.; Xu, H. Branched Silver Nanowires as Controllable Plasmon Routers. *Nano Lett.* **2010**, *10*, 1950–1954.
4. Solis, D.; Chang, W.-S.; Khanal, B. P.; Bao, K.; Nordlander, P.; Zubarev, E. R.; Link, S. Bleach-Imaged Plasmon Propagation (BlIPP) in Single Gold Nanowires. *Nano Lett.* **2010**, *10*, 3482–3485.
5. Ditlbacher, H.; Hohenau, A.; Wagner, D.; Kreibig, U.; Rogers, M.; Hofer, F.; Aussenegg, F. R.; Krenn, J. R. Silver Nanowires as Surface Plasmon Resonators. *Phys. Rev. Lett.* **2005**, *95*, 257403.
6. Akimov, A. V.; Mukherjee, A.; Yu, C. L.; Chang, D. E.; Zibrov, A. S.; Hemmer, P. R.; Park, H.; Lukin, M. D. Generation of Single Optical Plasmons in Metallic Nanowires Coupled to Quantum Dots. *Nature* **2007**, *450*, 402–406.
7. Knight, M. W.; Grady, N. K.; Bardhan, R.; Hao, F.; Nordlander, P.; Halas, N. J. Nanoparticle-Mediated Coupling of Light into a Nanowire. *Nano Lett.* **2007**, *7*, 2346–2350.
8. Aeschlimann, M.; Bauer, M.; Bayer, D.; Brixner, T.; Garcia de Abajo, F. J.; Pfeiffer, W.; Rohmer, M.; Spindler, C.; Steeb, F. Adaptive Subwavelength Control of Nano-Optical Fields. *Nature* **2007**, *446*, 301–304.
9. Cao, L.; Nome, R. A.; Montgomery, J. M.; Gray, S. K.; Scherer, N. F. Controlling Plasmonic Wave Packets in Silver Nanowires. *Nano Lett.* **2010**, *10*, 3389–3394.
10. Belardini, A.; Larciprete, M. C.; Centini, M.; Fazio, E.; Sibilia, C.; Chiappe, D.; Martella, C.; Toma, A.; Giordano, M.; de Mongeot, F. B. Circular Dichroism in the Optical Second-Harmonic Emission of Curved Gold Metal Nanowires. *Phys. Rev. Lett.* **2011**, *107*, 257401.
11. Guo, X.; Qiu, M.; Bao, J.; Wiley, B. J.; Yang, Q.; Zhang, X.; Ma, Y.; Yu, H.; Tong, L. Direct Coupling of Plasmonic and Photonic Nanowires for Hybrid Nanophotonic Components and Circuits. *Nano Lett.* **2009**, *9*, 4515–4519.
12. Agarwal, R.; Ladavac, K.; Roichman, Y.; Yu, G. H.; Lieber, C. M.; Grier, D. G. Manipulation and Assembly of Nanowires with Holographic Optical Traps. *Opt. Express* **2005**, *13*, 8906–8912.
13. Pauzauskie, P. J.; Radenovic, A.; Trepagnier, E.; Shroff, H.; Yang, P. D.; Liphardt, J. Optical Trapping and Integration of Semiconductor Nanowire Assemblies in Water. *Nat. Mater.* **2006**, *5*, 97–101.
14. Svoboda, K.; Block, S. M. Optical Trapping of Metallic Rayleigh Particles. *Opt. Lett.* **1994**, *19*, 930–932.
15. Prikulis, J.; Svedberg, F.; Käll, M.; Enger, J.; Ramser, K.; Goksor, M.; Hanstorp, D. Optical Spectroscopy of Single Trapped Metal Nanoparticles in Solution. *Nano Lett.* **2004**, *4*, 115–118.
16. Selhuber-Unkel, C.; Zins, I.; Schubert, O.; Soennichsen, C.; Oddershede, L. B. Quantitative Optical Trapping of Single Gold Nanorods. *Nano Lett.* **2008**, *8*, 2998–3003.
17. Toussaint, K. C., Jr.; Liu, M.; Pelton, M.; Pesic, J.; Guffey, M. J.; Guyot-Sionnest, P.; Scherer, N. F. Plasmon Resonance-Based Optical Trapping of Single and Multiple Au Nanoparticles. *Opt. Express* **2007**, *15*, 12017–12029.
18. Bosanac, L.; Aabo, T.; Bendix, P. M.; Oddershede, L. B. Efficient Optical Trapping and Visualization of Silver Nanoparticles. *Nano Lett.* **2008**, *8*, 1486–1491.
19. Hajizadeh, F.; Reihani, S. N. S. Optimized Optical Trapping of Gold Nanoparticles. *Opt. Express* **2010**, *18*, 551–559.
20. Pelton, M.; Liu, M. Z.; Kim, H. Y.; Smith, G.; Guyot-Sionnest, P.; Scherer, N. E. Optical Trapping and Alignment of Single Gold Nanorods by Using Plasmon Resonances. *Opt. Lett.* **2006**, *31*, 2075–2077.
21. Ruijgrok, P. V.; Verhart, N. R.; Zijlstra, P.; Tchebotareva, A. L.; Orrit, M. Brownian Fluctuations and Heating of an Optically Aligned Gold Nanorod. *Phys. Rev. Lett.* **2011**, *107*, 037401.
22. Jones, P. H.; Palmisano, F.; Bonaccorso, F.; Gucciardi, P. G.; Calogero, G.; Ferrari, A. C.; Maragó, O. M. Rotation

Detection in Light-Driven Nanorotors. *ACS Nano* **2009**, *3*, 3077–3084.
23. Tong, L.; Miljkovic, V. D.; Käll, M. Alignment, Rotation, and Spinning of Single Plasmonic Nanoparticles and Nanowires Using Polarization Dependent Optical Forces. *Nano Lett.* **2010**, *10*, 268–273.
24. Grigorenko, A. N.; Roberts, N. W.; Dickinson, M. R.; Zhang, Y. Nanometric Optical Tweezers Based on Nanostructured Substrates. *Nat. Photonics* **2008**, *2*, 365–370.
25. Jamshidi, A.; Pauzauskie, P. J.; Schuck, P. J.; Ohta, A. T.; Chiou, P.-Y.; Chou, J.; Yang, P.; Wu, M. C. Dynamic Manipulation and Separation of Individual Semiconducting and Metallic Nanowires. *Nat. Photonics* **2008**, *2*, 85–89.
26. Dienerowitz, M.; Mazilu, M.; Dholakia, K. Optical Manipulation of Nanoparticles: A Review. *J. Nanophotonics* **2008**, *2*, 021875–32.
27. Link, S.; El-Sayed, M. A. Spectral Properties and Relaxation Dynamics of Surface Plasmon Electronic Oscillations in Gold and Silver Nanodots and Nanorods. *J. Phys. Chem. B* **1999**, *103*, 8410–8426.
28. N'Gom, M.; Ringnalda, J.; Mansfield, J. F.; Agarwal, A.; Kotov, N.; Zaluzec, N. J.; Norris, T. B. Single Particle Plasmon Spectroscopy of Silver Nanowires and Gold Nanorods. *Nano Lett.* **2008**, *8*, 3200–3204.
29. Friese, M. E. J.; Nieminen, T. A.; Heckenberg, N. R.; Rubinsztein-Dunlop, H. Optical Alignment and Spinning of Laser-Trapped Microscopic Particles. *Nature* **1998**, *394*, 348–350.
30. Garces-Chavez, V.; McGloin, D.; Melville, H.; Sibbett, W.; Dholakia, K. Simultaneous Micromanipulation in Multiple Planes Using a Self-Reconstructing Light Beam. *Nature* **2002**, *419*, 145–147.
31. Arlt, J.; Garces-Chavez, V.; Sibbett, W.; Dholakia, K. Optical Micromanipulation Using a Bessel Light Beam. *Opt. Commun.* **2001**, *197*, 239–245.
32. Pelton, M.; Ladavac, K.; Grier, D. G. Transport and Fractionation in Periodic Potential-Energy Landscapes. *Phys. Rev. E* **2004**, *70*, 031108.
33. Guffey, M. J.; Scherer, N. F. All-Optical Patterning of Au Nanoparticles on Surfaces Using Optical Traps. *Nano Lett.* **2010**, *10*, 4302–4308.
34. Guffey, M. J.; Miller, R. L.; Gray, S. K.; Scherer, N. F. Plasmon-Driven Selective Deposition of Au Bipyramidal Nanoparticles. *Nano Lett.* **2011**, *11*, 4058–4066.
35. Korte, K. E.; Skrabalak, S. E.; Xia, Y. Rapid Synthesis of Silver Nanowires through a CuCl- or CuCl(2)-Mediated Polyol Process. *J. Mater. Chem.* **2008**, *18*, 437–441.
36. Crocker, J. C.; Grier, D. G. Methods of Digital Video Microscopy for Colloidal Studies. *J. Colloid Interface Sci.* **1996**, *179*, 298–310.
37. Johnson, P. B.; Christy, R. W. Optical Constants of the Noble Metals. *Phys. Rev. B* **1972**, *6*, 4370–4379.